ISSN 0031-918X, Physics of Metals and Metallography, 2022, Vol. 123, No. 1, pp. 32–36. © Pleiades Publishing, Ltd., 2022.
Russian Text © The Author(s), 2022, published in Fizika Metallov i Metallovedenie, 2022, Vol. 123, No. 1, pp. 35–39.

STRUCTURE, PHASE TRANSFORMATIONS, AND DIFFUSION

Changes in the Phase Composition of High-Manganese Steels during Tensile Deformation

M. A. Gervasyev[a], *, S. Kh. Estemirova[a, b], A. N. Mushnikov[c], V. A. Sharapova[a], A. A. Gusev[a], and M. A. Bashirova[a]

[a] *Ural Federal University named after the first President of Russia B.N. Yeltsin, Ekaterinburg, 620002 Russia*
[b] *Institute of Metallurgy, Ural Branch of the Russian Academy of Sciences, Ekaterinburg, 620016 Russia*
[c] *Institute of Engineering Science, Ural Branch of the Russian Academy of Sciences, Ekaterinburg, 620049 Russia*
**e-mail: m.a.gervasyev@urfu.ru*

Received February 17, 2021; revised September 14, 2021; accepted September 17, 2021

Abstract—High manganese steels with different contents of carbon and additionally alloyed with silicon are investigated. Mechanical properties of the steels under tensile deformation are determined, and the changes in their phase compositions are studied. The phase compositions of steels after quenching and after quenching with subsequent deformation are investigated by the X-ray diffraction method. Magnetometric measurements are performed directly during tensile deformation. It is shown that deformation has a different effect on the phase composition of steels, namely: in steel 40G20, a small amount of strain martensite is formed as a result of deformation; in steel 25G20S3, a substantial part of austenite undergoes a martensitic transformation ($\gamma \rightarrow \varepsilon$).

Keywords: austenitic steel, tensile deformation, X-ray structural analysis, magnetometry, phase composition
DOI: 10.1134/S0031918X22010057

INTRODUCTION

High-manganese austenitic steels have been known for over a hundred years [1]. High-manganese austenitic steels are widely used as wear-resistant materials [2, 3]. In addition, they exhibit a high cavitation resistance, a lower tendency to swelling upon irradiation, and a relatively low cost [4, 5]. Interest in such steels has increased in recent years, since they have begun being used as structural materials with a unique combination of strength and plasticity [6–8]. In particular, they are being used in the automotive industry as high-strength steels for deep drawing [9].

Deformation of high-manganese steels is accompanied by substantial transformation induced plasticity (TRIP) and twinning induced plasticity (TWIP) effects [10, 11]. These kinds of steels are characterized by a low yield point, a high strain-hardening rate, and a high ultimate strength. Deformation proceeds with little or no necking, with low tapering, and relatively high elongation. This ensures their high plasticity and strong hardening upon cold plastic deformation.

Deformation can be induced in Fe–Mn steels by various mechanisms depending on the energy of stacking fault (SFE), such as slipping, twinning, and the formation of strain martensite [12–17].

It should be noted that the formation of the following two types of martensite is possible in austenitic Fe–Mn steels: ε-martensite with a hexagonal lattice and α'-martensite with a cubic lattice. Different types of martensites determine different structures and strain hardening of steels [4, 5, 14].

It is known [18–22] that the content of ferromagnetic phases (ferrite, quenched α-martensite, and strain α'-martensite) can be estimated from the magnetic characteristics of a material.

The magnetometric method makes it possible to study changes in the phase composition directly in the process of deformation [23]. However, there are no such studies published for Fe–Mn–C alloys, which are promising structural materials.

MATERIALS AND TECHNIQUES

For the study, two austenitic high manganese steels 40G20 and 25G20S3 were taken (Table 1). The use of different contents of carbon and additional alloying with silicon made it possible to obtain steels with different stacking-fault energies (SFEs) that change the deformation mechanism of steels [12, 15, 16]. According to the published data, the SFE [10, 12, 13] of the investigated steels is approximately 20 MJ/m^2 for steel 40G20 and 13 MJ/m^2 for steel 25G20S3.

The changes in the phase compositions of the initial state (quenching from 1050°C in water) and after tensile deformation were studied by the X-ray powder diffraction (XRD) method on an XRD-7000 X-ray

diffractometer. The phases were identified using the PDF-2 database of the International Center for Diffraction Data (ICDD). In addition, magnetometric studies were performed directly in the process of tensile deformation using a Remagraph C-500 device, and the amount of the magnetic phase was calculated from these data. Mechanical tests of samples were performed on a Tinius OLsen SL-60 device at room temperature.

EXPERIMENTAL RESULTS

An analysis of the XRD data showed that both studied steels have an austenitic structure after quenching from 1050°C into water (initial state). At the same time, traces of the ε-phase (about 1%)—which could appear during the preparation of samples—were found in steel 25G20S3.

Tensile tests made it possible to obtain the following mechanical properties (Table 2). The steels under study exhibit high plasticity: their deformation begins at relatively low stresses, and their destruction occurs at relatively high stresses. This indicates a high strain hardening rate of the studied steels. However, deformation in these steels is induced by different mechanisms, which gives rise to a difference in the level of mechanical properties [17]. For the steels under study, large uniform elongation is observed; as a result, the samples are destroyed practically without necking (TRIP and TWIP effects). This is also evidenced by the low level of tapering.

Table 1. Chemical compositions of steels under study, wt %

Steel	C	Si	Mn	P	S	Cr	Ni
40G20	0.40	0.22	20.04	0.015	0.017	1.10	0.13
25G20S3	0.25	3.15	20.65	0.018	0.018	1.07	0.19

Table 2. Mechanical properties of steels under study

Steel	$\sigma_{0.2}$, MPa	σ_{UTS}, MPa	δ, %	ψ, %
40G20	270	780	38	24
25G20S3	320	850	30	17

Using the XRD method, X-ray diffraction patterns were obtained in different places of the samples after destruction, namely, in the immediate vicinity of the place of destruction and at a distance of 13 cm from it (see Figs. 1 and 2, respectively)

Based on the X-ray phase analysis results, the phase compositions of the studied high-manganese steels after tensile defromation were determined. The results of the performed experiment are given in Table 3.

The chemical composition of steels has a dramatic effect on the phase composition after deformation.

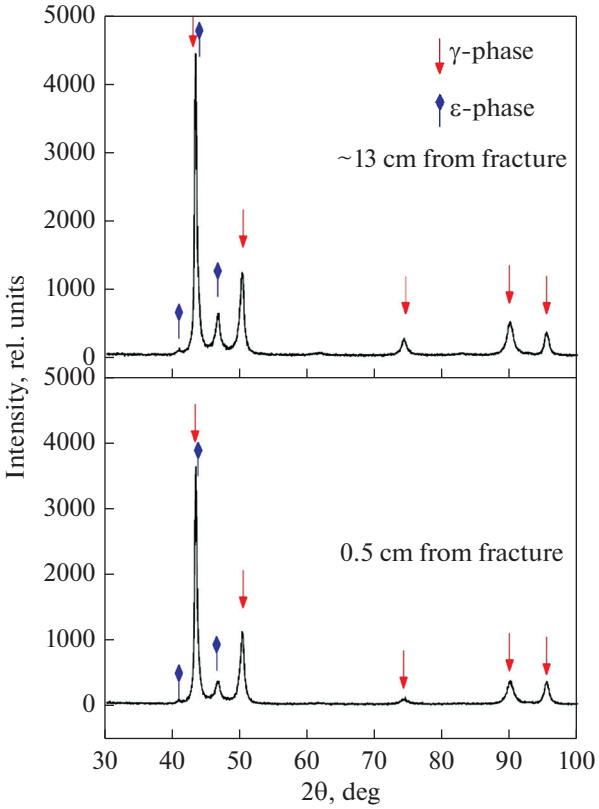

Fig. 1. Diffraction pattern of steel 40G20 after tensile deformation.

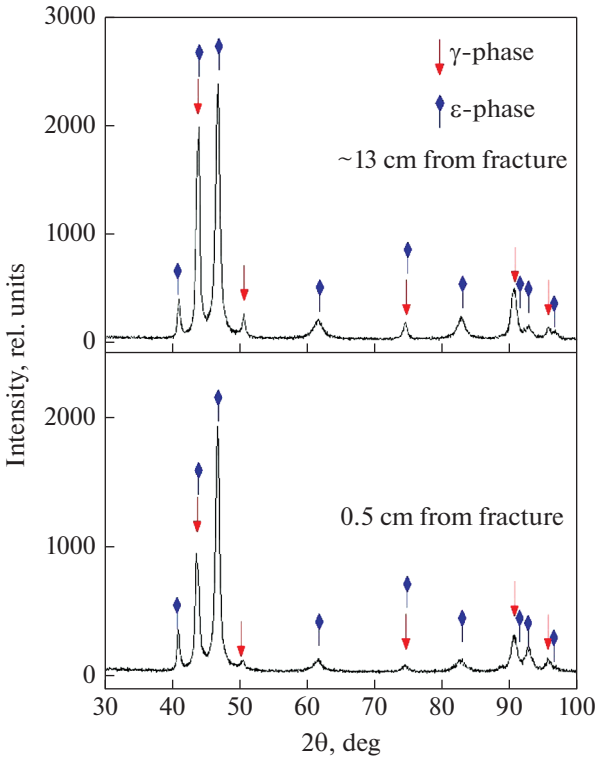

Fig. 2. Diffraction pattern for steel 25G20S3 after tensile deformation.

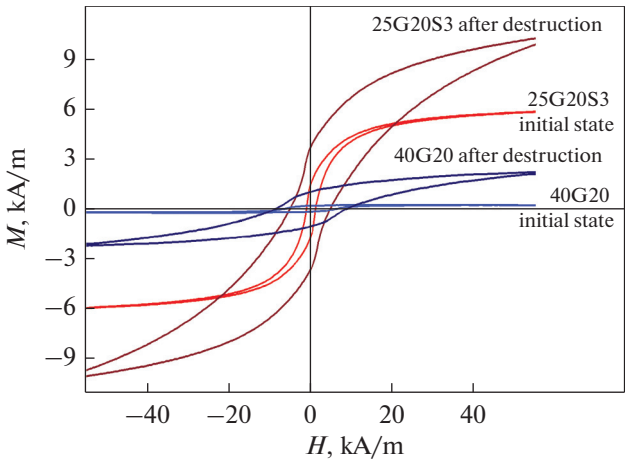

Fig. 3. Magnetic hysteresis loops of steels in the initial state and after destruction.

This indicates a change in the deformation mechanism. A small amount of ε-martensite (6%) was found in steel 40G20. In steel 25G20S3, a substantial part of the austenite present in the material transforms into the ε-phase. In steel 25G20S3, the intense formation of strain ε-martensite is observed (90–95%).

Table 3. Phase composition of steels after deformation, vol %

Steel	Sample cutting location relative to fracture location, cm	γ	ε
40G20	13	94	6
	0.5	94	6
25G20S3	13	10	90
	0.5	5	95

It should be noted that the phase composition after deformation is nearly the same in different parts of the sample, which indicates a uniform deformation process along the entire length of the sample due to plasticity induced by transformation or twinning. The presence of α'-martensite after deformation was not revealed by the XRD methods. This is due to the fact that the XRD lines are substantially broadened after deformation and do not allow one to detect small amounts of the α' phase.

To determine the amount of the magnetic α' phase, magnetometric mesurements were performed directly during tensile deformation. At each time point of the test, magnetic hysteresis loops were constructed (the initial and final loops are shown in Fig. 3).

The coercive force is the main structurally sensitive magnetic characteristic. Key magnetic characteristics of the material, such as coercive force H_c, residual induction B_r, and saturation magnetization M_s, are determined. The results are compiled in Table 4.

As can be seen from Table 4, the coercive force in steel 25G20S3 is substantially higher than that in steel 40G20. This is due to the formation of a large amount of ε-martensite during deformation in the former steel and, as a result, a high concentration of defects in this alloy.

An increase in the residual magnetic induction upon deformation is mainly caused by an increase in the content of the magnetic phase. To analyze the properties of this phase, one can consider such a parameter as the ratio of the residual magnetic induction to the saturation magnetization. It follows from Table 4 that this ratio is initially slightly higher in steel 40G20. This may be related to the influence of the

Table 4. Changes in the magnetic characteristics of steels after deformation

Strain, %	H_c, A/cm	B_r, T	M_s, A/m	$B_r/(\mu_0 M_s)$
		Steel 40G20		
0	1.8	2.28×10^{-4}	2.43×10^{2}	0.75
0.1	1.8	2.31×10^{-4}	2.78×10^{2}	0.66
7.3	2.8	3.92×10^{-4}	8.79×10^{2}	0.35
14.2	3.7	5.52×10^{-4}	1.36×10^{3}	0.32
27.3	6.7	1.12×10^{-3}	2.76×10^{3}	0.32
37.9	9.7	1.78×10^{-3}	3.10×10^{3}	0.46
		Steel 25G20S3		
0	7.3	1.96×10^{-3}	5.92×10^{3}	0.26
9.9	7.1	3.13×10^{-3}	6.56×10^{3}	0.38
14.4	7.7	3.53×10^{-3}	7.70×10^{3}	0.37
22.3	9.7	4.78×10^{-3}	1.08×10^{4}	0.35
29.9	13.4	7.13×10^{-3}	1.58×10^{4}	0.36

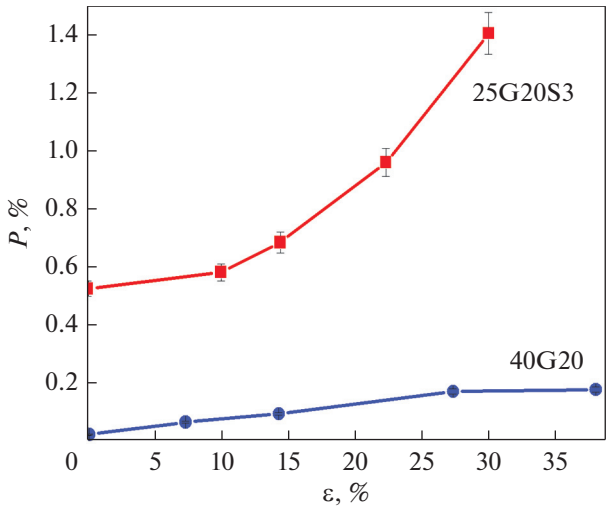

Fig. 4. Changes in the amount of the magnetic phase in the process of tensile deformation.

nonferromagnetic phases (γ and ε) on the magnetic properties.

The saturation magnetization in steel 25G20S3 is also higher at all deformation stages.

Using the test results and considering the magnetic characteristics of the material, concentration P of the magnetic phase, i.e., α-martensite, was calculated by formula

$$P = \frac{M_s}{M_{mag}} \times 100\%, \quad (1)$$

where M_{mag} denotes the theoretical saturation magnetization that a material consisting of only one ferromagnetic phase would have. An empirical formula was proposed in [21, 22] for the specific saturation magnetization of a multicomponent alloy, which is expressed through its chemical composition as follows:

$$\begin{aligned} M_{mag} &= 1.72\times10^6 - 2.19\times10^4(\mathrm{Cr}) \\ &- 2.63\times10^4(\mathrm{Ni}) - 2.23\times10^4(\mathrm{Mn}) \\ &- 4.85\times10^4(\mathrm{Si}) - 3.98\times10^4(\mathrm{P}) \\ &- 7.96\times10^3(\mathrm{C}) \pm 2.39\times10^4 \ \mathrm{A/m}, \end{aligned} \quad (2)$$

where the contents of chemical elements in the solid solution of the alloy under study are indicated in parentheses.

Using formula (2), we obtain $M_{mag} = 1.23 \times 10^6$ A/m for steel 40G20 and $M_{mag} = 1.08 \times 10^6$ A/m for steel 25G20S3.

Figure 4 shows the change in the amount of the α phase. As can be seen from Fig. 4, a very small amount of the magnetic phase is formed during standard mechanical tests. Substantially larger amounts of this phase are formed in steel 25G20S3 (up to 1.5%). It is well known [4, 5] that α'-martensite in high-manganese steels is formed in place of ε-martensite. As has been established in this study, a large amount of ε-martensite (90%) in steel 25G20S3 with a reduced energy of stacking-fault defects is formed with relatively low degrees of deformation under uniaxial tension. In steel 40G20, a small amount of α'-martensite is formed (less than 0.2%).

CONCLUSIONS

Magnetometric measurements performed in this study directly during tensile deformation and X-ray diffraction studies before and after test runs have made it possible to clarify the features of phase transformations that take place in the process of deformation of Fe–Mn–Si–C alloys.

In austenitic steel 40G20, the deformation process is accompanied by the formation of strain ε-martensite in a relatively small amount up to 6%. The formation of strain α-martensite is detected in a very small amount (0.2%).

In steel 25G20S3, intense formation of strain ε-martensite (90–95%) takes place, and strain α'-martensite (1.5%) is also formed.

The amount of strain α'-martensite is proportional to the amount of ε-martensite, which confirms the following sequence of formation of phases in the tensile deformation process: $\gamma \rightarrow \varepsilon \rightarrow \alpha'$.

The study of the phase compositions near the fracture and at a considerable distance from it has shown that the steel samples have practically the same phase composition. This indicates uniformity of deformation over the sample length, which is a consequence of plasticity induced by transformation or twinning.

CONFLICT OF INTEREST

The authors declare that they have no conflicts of interest.

REFERENCES

1. R. A. Hadfield, "Hadfield's manganese steel," Science **12**, No. 306, 284–286 (1888).
2. M. A. Filippov, A. A. Filipenkov, and G. M. Plotnikov, *Wear-Resistant Steels for Castings* (USTU-UPI, Yekaterinburg, 2009) [in Russian].
3. L. G. Korshunov, "Structural transformations during friction and wear resistance of austenitic steels," Fiz. Met. Metalloved., No. 8, 3–21 (1992).
4. I. N. Bogachev and V. F. Egolaev, *Structure and Properties of Ferromanganese Alloys* (Metallurgiya, Moscow, 1973) [in Russian].
5. V. V. Sagaradze and A. I. Uvarov, *Strengthening and Properties of Austenitic Steels* (RIO UrO RAN, Yekaterinburg, 2013) [in Russian].
6. O. Bouaziz, H. Zurob, B. Chehab, J. D. Embury, S. Allain, and M. Huang, "Effect of chemical composition on work hardening of Fe–Mn–C TWIP-steels," Mater. Sci. Technol. **27**, No. 3, 707–709 (2011).

7. X. Liang, J. R. McDermid, O. Bouaziz, X. Wang, J. D. Embury, and H. S. Zurob, "Microstructural evolution and strain hardening of Fe–24Mn and Fe–30Mn alloys during tensile deformation," Acta Mater. **57**, No. 13, 3978–3988 (2009).
8. M. Eskandari, M. A. Mohtadi-Bonab, A. Zarei-Hanzaki, J. A. Szpunar and R. Basu, "Texture and microstructure development of tensile deformed high-Mn steel during early stage of recrystallization," Phys. Met. Metallogr. **120**, No. 1, 32–40 (2019).
9. I. Yu. Pyshmintsev, *Strengthening of Sheet Steel for Cold Forming* (USTU-UPI, Yekaterinburg, 2004) [in Russian].
10. M. Koyamata, T. Sawaguchi, T. Lee, Ch. S. Lee, and K. Tsuzaki, "Work hardening assotiated with ε-martensitic transformation, deformation twinning and dynamic strain aging in Fe–17Mn–0.6C and Fe–17Mn–0.8C TWIP steels," Mater. Sci. Eng., A **528**, No. 24, 7310–7316 (2011).
11. B. C. De Cooman, Yu. Estrin, and S. K. Kim, "Twinning induced plasticity (TWIP) steels," Acta Mater. **142**, 283–362 (2018).
12. D. T. Pierce, J. A. Jimenez, J. Bentley, D. Raabe, and J. E. Witting, "The influence of stacking fault energy of the microstructural and strain hardening evolution of Fe–Mn–Al–Si steels during tensile deformation," Acta Mater. **100**, 178–190 (2015).
13. S. Curtze and V. -T. Kuokkala, "Dependence of tensile deformation behavior of TWIP steels on stacking fault energy, temperature and strain rate," Acta Mater. **58**, No. 15, 5129–5141 (2010).
14. J. Talonen, P. Aspegren, and H. Hanninen, "Comparison of different methods for measuring strain induced martensite content in austenitic steels," Mater. Sci. Technol. **20**, 1506–1512 (2004).
15. J. K. Kim and B. C. De Cooman, "Stacking fault energy and deformation mechanisms in Fe–*x*Mn–0.6C–*y*Al TWIP steel," Mater. Sci. Eng., A **676**, 216–231 (2016).
16. D. T. Pierce, J. Bentley, J. A. Jimenez, and J. E. Witting, "Stacking fault energy of measurements of Fe–Mn–Al–Si austenitic twinning induced plasticity steels," Scr. Mater. **66**, 753–756 (2012).
17. M. A. Gervas'ev, V. A. Khotinov, N. N. Ozerets, M. S. Khadyev, M. A. Bashirova, and A. A. Gusev, "Changes in microstructure and strain hardening of high-manganese steels under tension," Met. Sci. Heat Treat. **62**, 183–187 (2020).
18. M. N. Mikheev and E. S. Gorkunov, *Magnetic Methods of Structural Analysis and Non-Destructive Testing* (Nauka, Moscow, 1993) [in Russian].
19. M. S. Ogneva, M. B. Rigmant, N. V. Kazantseva, D. I. Davydov, and M. K. Korkh, "Effect of deformation martensite on the electrical and magnetic properties of plastically deformed chromium–nickel steel," Russ. J. Nondestr. Test. **53**, No. 9, 644–651 (2017).
20. M. K. Korkh, M. B. Rigmant, E. Yu. Sazhina, and A. V. Kochnev, "Measuring ferromagnetic phase content based on magnetic properties in two-phase chromium–nickel steels," Russ. J. Nondestr. Test. **55**, No. 11, 837–850 (2019).
21. Merinov P., Entin S., Beketov B., Runov A., "The magnetic testing of the ferrite content of austenitic stainless steel weld metal," NDT Int. **11**, 9–14 (1978).
22. P. E. Merinov and A. G. Mazepa, "Determination of deformation martensite in austenitic steels by the magnetic method," Zavod. Lab., No. 3, 47–49 (1997).
23. E. S. Gorkunov, S. V. Gladkovskii, S. M. Zadvorkin, S. Yu. Mitropol'skaya, and D. I. Vichuzhanin, "Evolution of magnetic properties of Fe–Mn and Fe–Mn–Cr steels with different stability of austenite during plastic deformation," Phys. Met. Metallogr. **105**, No. 4, 343–350 (2008).

Translated by O. Kadkin